The Formation of the Orientale Multi-Ring Basin: A Case Study of iSALE Modeling.
B. C. Johnson[1]*, J. C. Andrews-Hanna[2], G. S. Collins[3], H. J. Melosh[4], J. W. Head[1], D. M. Blair[5], A. M. Freed[4], K. Miljković[5], J. M. Soderblom[5], M. T. Zuber[5], [1] Department of Earth, Environmental and Planetary Sciences, Brown University, Providence, RI 02912, USA. (*Brandon_Johnson@Brown.edu). [2]Department of Geophysics, Colorado School of Mines, Golden, CO 80401. [3]Dept. Earth Science and Engineering, Imperial College London, London SW7 2AZ, UK. [4]Department of Earth, Atmospheric, and Planetary Sciences, Purdue University, West Lafayette, IN 47907.[5]Department of Earth, Atmospheric and Planetary Sciences, Massachusetts Institute of Technology.

Introduction: We introduce the iSALE shock physics code and discuss its capabilities and limitations using the formation of Orientale as a case study. This includes comparisons to a range of observations and constraints. NASA's Gravity Recovery and Interior Laboratory (GRAIL) mission provides an unprecedented view of the Moon's subsurface [1], showing that large multi-ring basins dominate the stratigraphy, tectonics, and crustal structure of the Moon [2]. Orientale is the youngest and best-preserved lunar multi-ring basin, and target of GRAIL's extended mission [3]. In addition to debate about which of Orientale's rings corresponds to the transient crater rim crest, there are several competing theories describing ring formation [4-8]. Here we present the first numerical models that directly resolve the development of Orientale's topographic rings during crater formation. Our models indicate that none of the rings correspond to the transient crater and that ring formation is reasonably well described by the ring tectonic theory of multi-ring basin formation.

Methods: We model the formation of Orientale using the 2D version of iSALE, a multi-material, multi-rheology, finite difference, shock physics code [9,10]. Our models include several improvements over previous models of basin forming lunar impacts [11-13], allowing us to directly resolve the formation of Orientale's rings. We include a dilatancy model [14], which describes how porosity of geological materials increases as they are deformed and contributes to shear localization [15]. We find that a damage model that has a smoother transition from intact to fractured rock strength with increasing plastic strain also results in more strain localization [15]. Finally, for structures the size of Orientale, the curvature of the surface is important. Thus, we model impacts into a Moon-like spherical target in a central gravity field.

We assume a vertical impact of a dunite asteroid at a typical lunar impact velocity of 15 km/s. We vary the impactor diameter, pre-impact crustal thickness, and thermal structure, while trying to match ring locations and crustal thickness derived from GRAIL gravity and Lunar Orbiter Laser Altimeter (LOLA) topography. Because rock strength decreases as its melting temperature is approached [13], the assumed pre-impact thermal structure of the target body has the most significant effect on the formation of large impact basins [9-11, 16].

Results: Our best-fit model assumes a 64-km diameter impactor, a 14-K/km linear thermal gradient from a surface temperature of 300 K that rolls over to an adiabat at 1300 K, and a pre-impact crustal thickness of 52 km. Our model provides insight into how Orientale's rings form. Shortly after ejecta emplacement, as the transient crater collapses, the Outer Rook fault forms, followed by the Cordillera fault (Fig 1a). This is consistent with observations suggesting that the Cordillera formed after ejecta emplacement [8]. Our model predicts that both faults cut through the entire crust as listric normal faults. Figure 1a shows that each fault has a few km offset and average dip angles of 50–55° within the crust.

Our models indicate that the faults associated with the Outer Rook and Cordillera are the result of inward flow of warm weak mantle material during collapse of the transient crater. This flow of weaker underlying material pulls the cooler crust along with it, ultimately causing extensional faulting with large offsets far from the transient crater rim (R=195 km, radius when crater is has maximum volume). Thus, the Outer Rook and Cordillera form as result of transient crater collapse in a target with strength that decreases with depth. The importance of the weak underlying mantle material is consistent with ring tectonic theory of multi-ring basin formation [5]. However, ring tectonic theory predicts the location of a single ring fault [5] and is not applicable to formation of the Inner Rook.

The collapse of the central uplift, which produces a bulge of crustal material, is crucial to formation of the Inner Rook (Fig 1b). This is consistent with previous interpretations [6, 8] that the formation of Inner Rook is related to the formation of peak rings seen in smaller basins. A secondary phase of inward collapse modifies the topographic expression of the Inner Rook (Fig 1 b, c), distinguishing the formation of the Inner Rook from peak ring formation [17].

Over the following few hours, crustal material flows toward the basin center completely covering the impact melt pool. While the massive impact melt pool of Orientale may differentiate as it cools [18], this cap of relatively cool crustal material covering the basin center is important for mascon formation [13].

In addition to forming rings in approximately the correct locations, models with pre-impact crustal thicknesses that range from 48–52 km produce excellent fits to the azimuthally averaged crustal thickness

profile derived from GRAIL gravity and LOLA topography (Fig. 2). We prefer the model with pre-impact crustal thickness of 52 km because it produces a thicker cap of cool crustal material at the center of the basin (Fig 2). We recognize that the initial crustal thickness varied over the area of the enormous Orientale basin and that, coupled with the effects of a more realistic oblique impact, this may explain the marked difference between the development of rings in the eastern and western sectors of the basin.
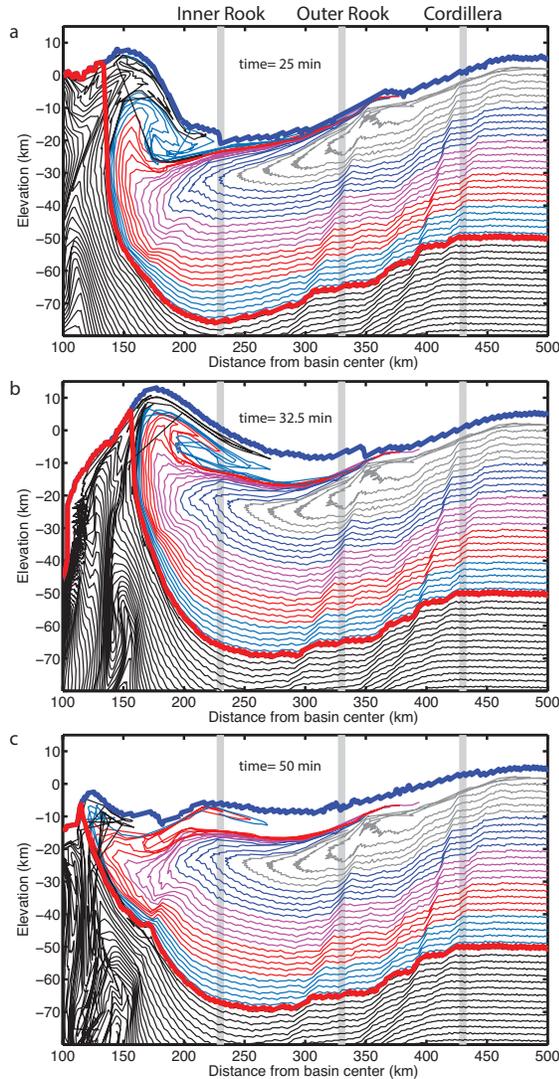
Figure 1. Vertically exaggerated, time series highlighting the Cordillera and Outer Rook faults, formation of the Inner Rook. Thin lines connect Lagrangian tracers that were at equal depth before the impact. In the crust, the color of tracer lines changes every 10 km in pre-impact depth. The thick blue and red curves mark model topography and crust mantle interface, respectively. The thick gray lines mark the observed surface locations of Orientale's ring. Elevation and distance are with respect to a sphere.

The modeled and observationally derived azimuthally averaged crustal thickness profiles both exhibit local minima in the crustal thickness at distances of about 300 km and 400 km from the basin center (Fig 2). These minima are the direct result of faults with few-km offsets cutting through the crust mantle interface. A single idealized planar fault, with a dip angle of 50 degrees and offset of 4 km, cutting through 50 km thick crust will create an ~40 km wide region where the crust is thinned by ~3 km. This idealized situation is very similar to the modeled Outer Rook (Fig 2, red curve between 300–340 km from basin center). When extension occurs close to a fault (within ~40 km) the zone of crustal thinning is broader (Fig 1, Fig 2). Regardless of their width, these local minima in crustal thickness as observed by GRAIL may reveal ring faults in highly degraded or mare filled basins.

References: [1] Zuber M. T. *et al.* (2013) *Science* 339, 668–671. [2] Wieczorek M. A. *et al.* (2013) *Science* 339, 671–675. [3] Zuber M. T. *et al.* (2014) *LPS VL,* 2061 [4] Baldwin, R. B. (1972). *PEPI* 6, 327–339. [5] Melosh H. J. and McKinnon W. B. (1978) *GRL* 5, 985–988 [6] Head J. W. (2010) *GRL* 37, L02203. [7] Hodges C. A. and Wilhelms D. E. (1978) *Icarus* 34, 294–323. [8] Head J.W. (1974) *The Moon* 11, 327–356. [9] Collins G. S. et al. (2004) *MAPS* 39, 217–231. [10] Wünnemann K. *et al.* (2006) *Icarus* 180, 514–527. [11] Potter R. W. K. *et al.* (2013) *JGR Planets* 118, 963–979. [12] Miljkovic K. *et al.* (2013) *Science* 342, 724–726 (2013). [13] Freed, A. M. *et al.* (2014) *JGR. Planets*, JE004657. [14] Collins G.S. (2014) *J. Geophys. Res. Planets*, JE004708. [15] Montési L. G. J. and Zuber M. T. (2002) *JGR (Solid Earth)* 107, 1–20. [16] Ivanov B. A. *et al.* (2010) *Geological Society of America Special Papers.* 465, 29–49. [17] Collins G. S. *et al.* (2002) *Icarus* 157, 24–33. [18] Vaughan W. M. *et al.* (2013) *Icarus* 223, 749–765.
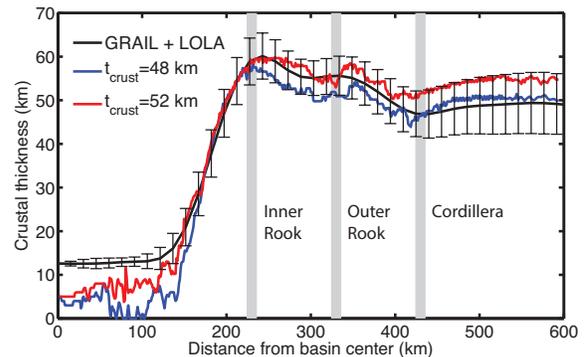
Figure 2. Crustal thickness profiles. Post-impact crustal thickness is plotted from the best-fit model (red) and for a model with a pre-impact crustal thickness of 48 km (blue). An azimuthally averaged profile of crustal thickness (black), derived from LOLA topography and GRAIL gravity, is shown for comparison. Error bars are 1-sigma deviations from the mean